A three-dimensional model study of the effect of new temperature-dependent quantum yields for acetone photolysis

S. R. Arnold and M. P. Chipperfield
Institute for Atmospheric Science, School of Earth and Environment, University of Leeds, Leeds, UK

M. A. Blitz
Department of Chemistry, University of Leeds, Leeds, UK

Received 21 March 2005; revised 21 July 2005; accepted 22 August 2005; published 22 November 2005.

[1] We have used the TOMCAT three-dimensional chemical transport model (CTM) to investigate the impact of recent laboratory measurements of the temperature dependence of the acetone photolysis quantum yield on global tropospheric chemistry. The new acetone quantum yields cause a significant decrease in the calculated acetone loss rate in troposphere. The annual global mean photolysis loss of acetone is reduced by a factor of ~2, making OH oxidation the dominant acetone sink. Photolysis rates decrease by between ~80 and 90% in the cold upper troposphere (UT). The atmospheric lifetime of acetone increases from 22 to 35 days, with an increase in the global burden from 2.6 to 4.1 Tg. This is maintained through a global source strength of 42.5 Tg/yr, which is approximately half of that inferred by some previous model studies. Comparisons of modeled and observed acetone profiles from the remote tropical Pacific demonstrate much improved agreement with the new quantum yields, with a reduction in the model bias relative to aircraft observations from −50 to −17%. With the new quantum yields, modeled peroxyacetylnitrate (PAN) decreases in the UT and throughout the Northern Hemisphere. PAN increases are modeled in Southern Hemisphere, as the increases in acetone outweigh the slower rate of peroxyacetyl production. The new quantum yields reduce the model HO_x(=OH + HO_2) throughout the troposphere. The locations of largest changes to HO_x and the OH:HO_2 ratio, caused by changes in NO_x, mean the impact on model global OH is small (−0.5%). The net effect of using the new quantum yields on tropospheric ozone is also small; the model predicts a maximum 1% decrease in the Northern Hemisphere lower troposphere.

Citation: Arnold, S. R., M. P. Chipperfield, and M. A. Blitz (2005), A three-dimensional model study of the effect of new temperature-dependent quantum yields for acetone photolysis, *J. Geophys. Res.*, *110*, D22305, doi:10.1029/2005JD005998.

1. Introduction

[2] The ubiquity of oxygenated volatile organic compounds (OVOC) throughout the global troposphere has been noted in several studies [e.g., *Singh et al.*, 1995, 2001, 2004; *Arnold et al.*, 1997]. The large abundance of OVOCs has consequences for the oxidizing capacity and ozone budget of the atmosphere, since their photo-oxidation leads to the efficient formation of radical species [*Carlier et al.*, 1986]. Such radical formation has been shown to be an important source of HO_x in the upper troposphere (UT) and can also lead to the sequestration of NO_x into radical nitrate species, such as peroxyacetylnitrate (PAN, $MeCO_3NO_2$) [*Singh et al.*, 1994, 1995; *Arnold et al.*, 1997; *McKeen et al.*, 1997; *Müller and Brasseur*, 1999; *Wennberg et al.*, 1998; *Jaeglé et al.*, 2000]. These species are effectively nitrogen reservoirs, acting as an efficient mechanism for the transport of reactive nitrogen to remote regions of the troposphere [*Singh and Hanst*, 1981].

[3] Acetone is one of the most abundant of the OVOCs, with free tropospheric concentrations ranging between 0.2 and more than 2 ppbv [*Singh et al.*, 1995, 2001, 2004; *Arnold et al.*, 1997; *Traub et al.*, 2003]. Studies of the large-scale acetone distribution in the troposphere have, to date, shown difficulty in reconciling observed large concentrations with its known sources and sinks [*Jacob et al.*, 2002; *Singh et al.*, 2004]. As a result, large uncertainties remain regarding the role of the ocean as a regional source or sink for acetone, as well as uncertainties regarding the magnitudes of natural, biomass, and anthropogenic emissions [*Jacob et al.*, 2002; *Singh et al.*, 2004].

[4] Recently, first measurements of a temperature dependence of the quantum yield for acetone photodissociation were found to decrease the acetone photolysis sink by a

Copyright 2005 by the American Geophysical Union.
0148-0227/05/2005JD005998$09.00

Table 1. Chemical Species in the CTM[a]

Category	Species
Shorter-lived species	O_x(= O_3 + $O(^3P)$ + $O(^1D)$), H_2O_2 NO_x(= NO + NO_2), NO_3, N_2O_5, HNO_3, HO_2NO_2, HONO $MeCO_3NO_2$, $EtCO_3NO_2$, $MeONO_2$ HCHO, MeOOH, MeCHO, Me_2CO, C_2H_6, EtOOH, EtCHO, C_3H_8, n-PrOOH, i-PrOOH,
Steady-state	OH, HO_2, MeO_2, EtO_2, $MeCO_3$, $EtCO_3$, n-PrOO, i-PrOO $MeCOCH_2OO$, $MeCOCH_2OOH$
Source gases	CH_4, CO
Fixed	O_2, N_2, H_2, CO_2
Analyses	H_2O

[a]Me = CH_3, Et = C_2H_5, Pr = C_3H_7.

factor of 2.5–10 in the UT [*Blitz et al.*, 2004]. Applying these new measurements to a photochemical box model demonstrated a large reduction in the impact of acetone on HO_x and NO_y chemistry in the midlatitude and tropical UT [*Arnold et al.*, 2004]. HO_x yields from acetone were reduced by between a factor of 2 and 4, and the acetone lifetime was significantly increased.

[5] In this paper we use a three-dimensional (3-D) chemical transport model to extend the study of *Arnold et al.* [2004]. Here we investigate the impact of the new quantum yields on the calculated photolysis and acetone distribution over all latitudes and seasons. We compare the modeled acetone with surface/aircraft data to investigate if the slower photolysis and longer acetone lifetime improves model/data agreement. We then investigate the impact of the changed modeled acetone on other species such as PAN, NO_x, HO_x, and ozone. Section 2 describes the TOMCAT model in some detail. The model results are presented in section 3.

2. TOMCAT 3-D Model

[6] In this study we have used the TOMCAT three-dimensional (3-D) off-line chemical transport model (CTM) [e.g., *Chipperfield et al.*, 1993; *Stockwell and Chipperfield* 1999]. The model is forced using winds, temperature, and humidity from meteorological analyses. Tracer advection by the resolved winds is performed using the scheme of *Prather* [1986]. In the updated version used here (M. P. Chipperfield, New version of the TOMCAT/SLIMCAT off-line chemical transport model, submitted to *Quarterly Journal of the Royal Meteorological Society*, 2005) subgrid scale transport is performed using the Tiedtke convection scheme [*Tiedtke*, 1989; *Stockwell and Chipperfield* 1999] and the *Holtslag and Boville* [1993] parameterization for turbulent mixing in the boundary layer following the method of *Wang et al.* [1999].

[7] In the past, TOMCAT has been used for studies of both the stratosphere and troposphere with both simple tracers and detailed chemistry. Studies with detailed tropospheric chemistry, as used here, have been described by, e.g., *Law et al.* [1998]. However, certain changes have been made to the tropospheric chemistry scheme for this study and so we now give complete details of model species, reactions, photolysis rate calculations, and emissions, which are all relevant to the aims of this study.

2.1. Chemical Scheme

[8] Table 1 lists the species now contained in the updated TOMCAT chemical scheme used here. The model uses 23 advected tracers (species and families). Short-lived species are not advected and assumed to be in photochemical steady-state (e.g., OH). The model H_2O field is taken from the analyses used to forced the model. The chemical reactions are listed in Tables 2–4. Wherever possible kinetic data is taken from IUPAC (http://www.iupac-kinetic.ch.cam.ac.uk) and for reactions not contained in this we use the Leeds Master Chemical Mechanism (MCM). The exceptions are reactions 41, 56, and 78 which are taken from *Sander et al.* [2003]. The chemistry is integrated using the ASAD scheme [*Carver et al.*, 1997].

2.2. Photolysis Scheme

[9] In previous TOMCAT tropospheric chemistry studies [e.g., *Law et al.*, 1998; *O'Connor et al.*, 2004] the model has used precalculated photolysis (J) rates based on the original code of *Hough* [1988] used in a 2-D latitude-height model. Within TOMCAT these photolysis rates were interpolated to the local solar time but there was no other coupling with the local model 3-D fields. This study requires interactive photolysis rates and therefore we have again used the code of *Hough* [1988] but now inserted it into TOMCAT.

[10] The scheme of *Hough* [1988] is based on the two-stream approach which considers the direct and scattered beam. The scheme considers six orders of isotropic scattering. A climatological cloud field is specified. The version used here has 203 wavelength bins from 121 nm to 850 nm. Within TOMCAT the J rates are calculated at every chemical time step (15 min) using the model profiles of temperature and ozone in the calculation of cross sections, quantum yields, and solar flux, where appropriate. Where possible, photochemical data has been updated from *Sander et al.* [2003]. The photolysis scheme used here in TOMCAT is very similar to that used in the box model study of *Arnold et al.* [2004].

[11] Overall, the photolysis scheme has not changed significantly and the model is expected to behave similarly to the previous validated versions [e.g., *Law et al.*, 1998]. Small differences are expected in photolysis rate values, as model fields (e.g., T) are now used interactively, and we have specified fields of surface albedo and clouds and have updated the photochemical data. Figure 1 shows some comparisons of CO and ozone profiles from around the globe to demonstrate the similarity of the old and new model schemes. The main difference between the two simulations is that the new photolysis treatment gives a more oxidizing troposphere, slightly reducing CO and increasing ozone concentrations. This is also noted in section 3.5 (below) in the discussion of the global mean OH and methane lifetime. Southern Hemisphere (SH) CO concentrations are overestimated. This has been noted in

Table 2. CTM Gas Phase Bimolecular Reactions[a]

Reaction	Reactants	Products
1	HO_2 + NO	→ OH + NO_2
2	HO_2 + NO_3	→ OH + NO_2
3	HO_2 + O_3	→ OH + O_2
4	HO_2 + HO_2	→ H_2O_2 + O_2
5	HO_2 + MeOO	→ MeOOH + O_2
6	HO_2 + EtOO	→ EtOOH + O_2
7a	HO_2 + $MeCO_3$	→ $MeCO_3H$ + O_2
7b	HO_2 + $MeCO_3$	→ $MeCO_2H$ + O_3
8	HO_2 + n-PrOO	→ n-PrOOH
9	HO_2 + i-PrOO	→ i-PrOOH
10a	HO_2 + $EtCO_3$	→ $EtCO_3H$ + O_2
10b	HO_2 + $EtCO_3$	→ $EtCO_2H$ + O_3
11	HO_2 + $MeCOCH_2OO$	→ $MeCOCH_2OOH$ + O_2
12a	MeOO + NO (+ O_2)	→ HO_2+ HCHO + NO_2
12b	MeOO + NO	→ $MeONO_2$
13	MeOO + NO_3	→ HO_2 + HCHO + NO_2
14a	MeOO + MeOO	→ MeOH + HCHO + O_2
14b	MeOO + MeOO	→ 2HO_2 + 2HCHO
15a	MeOO + $MeCO_3$	→ HO_2 + HCHO + MeOO
15b	MeOO + $MeCO_3$	→ $MeCO_2H$ + HCHO
16	EtOO + NO	→ MeCHO + HO_2 + NO_2
17	EtOO + NO_3	→ MeCHO + HO_2 + NO_2
18	EtOO + $MeCO_3$	→ MeCHO + HO_2 + MeOO
19	$MeCO_3$ + NO (+ O_2)	→ MeOO + CO_2 + NO_2
20	$MeCO_3$ + NO_3	→ MeOO + CO_2 + NO_2
21	$MeCO_3$ + n-PrOO	→ MeOO + EtCHO + HO_2
22	$MeCO_3$ + i-PrOO	→ MeOO + Me_2CO + HO_2
23	n-PrOO + NO	→ EtCHO + HO_2 + NO_2
24	n-PrOO + NO_3	→ EtCHO + HO_2 + NO_2
25	i-PrOO + NO	→ Me_2CO + HO_2 + NO_2
26	i-PrOO + NO_3	→ Me_2CO + HO_2 + NO_2
27	$EtCO_3$ + NO	→ EtOO + CO_2 + NO_2
28	$EtCO_3$ + NO_3	→ EtOO + CO_2 + NO_2
29	$MeCOCH_2OO$ + NO	→ $MeCO_3$ + HCHO + NO_2
30	$MeCOCH_2OO$ + NO_3	→ $MeCO_3$ + HCHO + NO_2
31	NO + NO_3	→ 2NO_2
32	NO + O_3	→ NO_2 + O_2
33	NO_2 + $O(^3P)$	→ NO + O_2
34	NO_2 + O_3	→ NO_3 + O_2
35	NO_3 + HCHO (+ O_2)	→ $HONO_2$ + HO_2 + CO
36	NO_3 + MeCHO	→ $HONO_2$ + $MeCO_3$
37	NO_3 + EtCHO	→ $HONO_2$ + $EtCO_3$
38	NO_3 + Me_2CO	→ $HONO_2$ + $MeCOCH_2OO$
39	N_2O_5 + H_2O	→ 2$HONO_2$
40	$O(^3P)$ + O_3	→ 2O_2
41a	$O(^1D)$ + CH_4	→ OH + MeOO
41b	$O(^1D)$ + CH_4	→ HCHO + H_2
41c	$O(^1D)$ + CH_4	→ HCHO +2HO_2
42	$O(^1D)$ + H_2O	→ 2OH
43	$O(^1D)$ + N_2	→ $O(^3P)$ + N_2
44	$O(^1D)$ + O_2	→ $O(^3P)$ + O_2
45	OH + CH_4	→ H_2O + MeOO
46	OH + C_2H_6	→ H_2O + EtOO
47a	OH + C_3H_8	→ n-PrOO + H_2O
47b	OH + C_3H_8	→ i-PrOO + H_2O
48	OH + CO	→ HO_2 + CO_2
49	OH + EtCHO	→ H_2O + $EtCO_3$
50a	OH + EtOOH	→ H_2O + MeCHO + OH
50b	OH + EtOOH	→ H_2O + EtOO
51	OH + H_2	→ H_2O + HO_2
52	OH + H_2O_2	→ H_2O + HO_2
53	OH + HCHO	→ H_2O + HO_2 + CO
54	OH + HO_2	→ H_2O + O_2
55	OH + HO_2NO_2	→ H_2O + NO_2
56	OH + $HONO_2$	→ H_2O + NO_3
57	OH + HONO	→ H_2O + NO_2
58a	OH + MeOOH	→ H_2O + HCHO + OH
58b	OH + MeOOH	→ H_2O + MeOO
59	OH + $MeONO_2$	→ HCHO + NO_2 + H_2O
60	OH + Me_2CO (+ O_2)	→ H_2O + $MeCOCH_2OO$
61	OH + $MeCOCH_2OOH$	→ H_2O + $MeCOCH_2OO$
62	OH + MeCHO	→ H_2O + $MeCO_3$
63	OH + NO_3	→ HO_2 + NO_2
64	OH + O_3	→ HO_2 + O_2
65	OH + OH	→ H_2O + $O(^3P)$
66	OH + $MeCO_3NO_2$	→ HCHO + NO_2 + H_2O
67	OH + $EtCO_3NO_2$	→ MeCHO + NO_2 + H_2O
68	OH + n-PrOOH	→ n-PrOO + H_2O
69	OH + n-PrOOH	→ EtCHO + H_2O + OH
70	OH + i-PrOOH	→ i-PrOO + H_2O
71	OH + i-PrOOH	→ Me_2CO + OH

[a]$MeCO_3H$, $MeCO_2H$, $EtCO_3H$, $EtCO_2H$, MeOH - not considered further by chemistry scheme.

comparisons of many other models and is attributed to an overestimate in SH CO sources from the IPCC emissions [*Prather et al.*, 2001].

2.3. Surface Emissions

[12] Table 5 gives the annual mean fluxes of the surface-emitted species in the model. These are based on earlier runs of TOMCAT except for acetone which has been updated based on IPCC scenarios (D. Stevenson, personal communication, 2004). The total surface emission flux of acetone specified in the model is 27 Tg/yr. This is composed of 20 Tg/yr from natural sources, 5 Tg/yr from biomass burning (distributed according to *van der Werf et al.* [2003]), and 5 Tg/yr from industrial sources (distributed according to *Dentener et al.* [2004]). Given large uncertainties in the role of the ocean as a source and sink of acetone [*Singh et al.*, 2001; *Jacob et al.*, 2002], we remove the impact of the ocean terms on the acetone budget by assuming a net zero acetone atmosphere-ocean flux. The model acetone source from alkane oxidation is around 16 Tg/yr, giving a total acetone source of around 43 Tg/yr. Owing to the lack of hydrocarbon complexity in the model scheme, oxidation of monoterpenes, methylbutanol, and higher iso-alkanes are not included as sources of acetone.

2.4. Model Experiments

[13] We have performed three 20-month simulations of TOMCAT to test the effect of the new quantum yields for acetone photolysis. The runs were initialized on 1 April 2000 and forced using ECMWF operational analyses. The model resolution was 5.6° × 5.6° horizontally with 31 hybrid σ-p levels from the surface to 10 hPa. Run **NQY** used the acetone quantum yields from the parameterization of *Blitz et al.* [2004], while run **RQY** used the standard yields from *Gierczak et al.* [1998]. For comparison a final simulation (**OLD**) was done with the pre-calculated J rate values used in previously published TOMCAT studies.

[14] The rate constant for the reaction of acetone with OH is $k = 8.8 \times 10^{-12}\exp(-1320/T) + 1.7 \times 10^{-14}\exp(420/T)$ (http://www.iupac-kinetic.ch.cam.ac.uk). Dry deposition of acetone was included in the model over land with a deposition velocity of 0.1 cm/s [*Jacob et al.*, 2002].

[15] The model output was saved every 3.75 days to allow precession of the diurnal cycle, avoiding regional bias in monthly mean fields. After a 6-month spin-up, the output

Table 3. CTM Gas Phase Termolecular and Thermal Decomposition Reactions

Reaction	Reactants	Products
72	$HO_2 + NO_2 + M$	$\rightarrow HO_2NO_2 + M$
73	$HO_2NO_2 + M$	$\rightarrow HO_2 + NO_2 + M$
74	$MeCO_3 + NO_2 + M$	$\rightarrow MeCO_3NO_2 + M$
75	$MeCO_3NO_2 + M$	$\rightarrow MeCO_3 + NO_2 + M$
76	$N_2O_5 + M$	$\rightarrow NO_2 + NO_3 + M$
77	$NO_2 + NO_3 + M$	$\rightarrow N_2O_5 + M$
78	$O(^3P) + O_2 + M$	$\rightarrow O_3 + M$
79	$OH + NO + M$	$\rightarrow HONO + M$
80	$OH + NO_2 + M$	$\rightarrow HONO_2 + M$
81	$OH + OH + M$	$\rightarrow H_2O_2 + M$
82	$EtCO_3 + NO_2 + M$	$\rightarrow EtCO_3NO_2 + M$
83	$EtCO_3NO_2 + M$	$\rightarrow EtCO_3 + NO_2 + M$

from months 7–20 was used to create monthly mean fields of the model tracers.

3. Three-Dimensional Model Results

[16] First, we investigate the direct impact of the new quantum yields on acetone photolysis. We then examine the changes to global tropospheric chemistry caused by these reductions to the acetone *J* rate.

3.1. Acetone Photolysis

[17] First, we examine the direct effect of the change in acetone quantum yields on the modeled acetone photolysis rates. The annual global mean acetone photolysis rate (Figure 2) reduces by 58%, from 3.93×10^{-7} to 1.64×10^{-7} s^{-1} on switching from **RQY** to **NQY**. The greatest fractional difference produced is in the winter UT of both hemispheres, with a reduction of up to ~90%. Reductions to the maximum acetone photolysis rate, in the summer lower-latitude UT, are on the order of ~70%, reducing a maximum *J* rate of more than 5.7×10^{-7} s^{-1} to less than 1.6×10^{-7} s^{-1}. As shown by *Blitz et al.* [2004], largest reductions to the photolysis rate are produced in the UT, where temperatures are lowest. However, in the warmest regions, near the surface in the tropics, fractional reductions to the *J* rate are still greater than 50%.

[18] Reductions to the acetone photolysis rate in the autumn UT of between 70 and 90% (not shown) are comparable with those calculated in the box model study of *Arnold et al.* [2004], which showed reductions of ~85% and ~60% to the *J* rate in the midlatitude and tropical UT, respectively.

3.2. Acetone Budget

[19] The zonal mean acetone distribution (Figure 3) shows largest concentrations at the surface in the Northern Hemisphere (NH) winter. This is due to the large NH source strength, coupled to the smallest *J* loss and OH concentrations during winter. Southern Hemisphere (SH) source strengths are far smaller, and consequently SH zonal-mean concentrations do not exceed 600 pptv. The largest SH concentrations occur in JJA near the surface, when loss through OH and photolysis are slowest. The maximum SH concentrations occur at lower latitudes where the strongest SH sources are located (see Figure 4). Acetone distributions in the tropics indicate efficient vertical transport of larger surface concentrations to higher altitudes, highlighting the potential key role of acetone in tropical UT HO_x production. Surface distributions (Figure 4) show strongest sources are associated with anthropogenic emissions (either directly or through oxidation of iso-alkanes) in NH midlatitudes and biomass burning sources in tropical Africa, Asia, and South America. Maximum surface concentrations of more than 5 ppbv are modeled in these source regions. A strong contrast is seen between mean surface NH concentrations between winter and spring (Figure 3) associated with the longer acetone lifetime in winter which facilitates long-range transport of relatively high acetone concentrations (>0.6 ppbv) to all NH latitudes. In contrast, owing to the smaller SH source strength, SH surface acetone concentrations do not exceed 0.5 ppbv at middle/high latitudes.

[20] Owing to the large reduction in acetone photolysis rates with **NQY**, zonal mean acetone concentrations are enhanced globally for all seasons and at all altitudes. Large fractional increases in SH acetone concentrations are seen, particularly in summer. The localized nature of SH sources and large increase to the acetone lifetime mean that acetone concentrations in remote SH regions are greatly enhanced by transport. Surface acetone concentrations are greatly enhanced in the remote SH regions and over the oceans.

[21] Table 6 shows global annual mean acetone budget terms for the three model runs. As noted in section 3.1, compared to the old precalculated *J* rate scheme (**OLD**), the **RQY** simulation produces a more photochemically active troposphere, increasing the photolysis loss of acetone from 17.0 to 18.2 Tg yr^{-1}. Photolysis, OH loss, and dry deposition account for 43%, 39%, and 17% of the acetone sink, respectively, in the **RQY** simulation, with a small (<1%) contribution from oxidation by NO_3. Loss via OH oxidation relative to photolysis is large compared to the study of *Jacob et al.* [2002] and is at the high end of estimates from *Singh et al.* [1994]. A larger *J* loss would require greater transport of acetone to higher altitudes, where photolysis loss dominates. The different relative strengths of OH and

Table 4. CTM Photolysis Reactions

Reaction	Reactants	Products
1	$EtOOH + h\nu (+ O_2)$	$\rightarrow MeCHO + HO_2 + OH$
2	$H_2O_2 + h\nu$	$\rightarrow OH + OH$
3a	$HCHO + h\nu (+ 2O_2)$	$\rightarrow HO_2 + HO_2 + CO$
3b	$HCHO + h\nu$	$\rightarrow H_2 + CO$
4	$HO_2NO_2 + h\nu$	$\rightarrow HO_2 + NO_2$
5	$HONO_2 + h\nu$	$\rightarrow OH + NO_2$
6a	$MeCHO + h\nu (+2O_2)$	$\rightarrow MeOO + HO_2 + CO$
6b	$MeCHO + h\nu$	$\rightarrow CH_4 + CO$
7	$MeOOH + h\nu (+ O_2)$	$\rightarrow HO_2 + HCHO + OH$
8	$N_2O_5 + h\nu$	$\rightarrow NO_3 + NO_2$
9	$NO_2 + h\nu$	$\rightarrow NO + O(^3P)$
10a	$NO_3 + h\nu$	$\rightarrow NO + O_2$
10b	$NO_3 + h\nu$	$\rightarrow NO_2 + O(^3P)$
11	$O_2 + h\nu$	$\rightarrow 2O(^3P)$
12a	$O_3 + h\nu$	$\rightarrow O_2 + O(^1D)$
12b	$O_3 + h\nu$	$\rightarrow O_2 + O(^3P)$
13	$MeCO_3NO_2 + h\nu$	$\rightarrow MeCO_3 + NO_2$
14	$HONO + h\nu$	$\rightarrow OH + NO$
15	$EtCHO + h\nu (+ 2O_2)$	$\rightarrow EtOO + HO_2 + CO$
16	$Me_2CO + h\nu (+2O_2)$	$\rightarrow MeCO_3 + MeOO$
17	$n\text{-}PrOOH + h\nu (+ O_2)$	$\rightarrow EtCHO + HO_2 + OH$
18	$i\text{-}PrOOH + h\nu (+ O_2)$	$\rightarrow Me_2CO + HO_2 + OH$
19	$MeCOCH_2OOH + h\nu (+ O_2)$	$\rightarrow MeCO_3 + HCHO + OH$
20	$EtCO_3NO_2 + h\nu$	$\rightarrow EtCO_3 + NO_2$
21	$MeONO_2 + h\nu (+ O_2)$	$\rightarrow HO_2 + HCHO + NO_2$

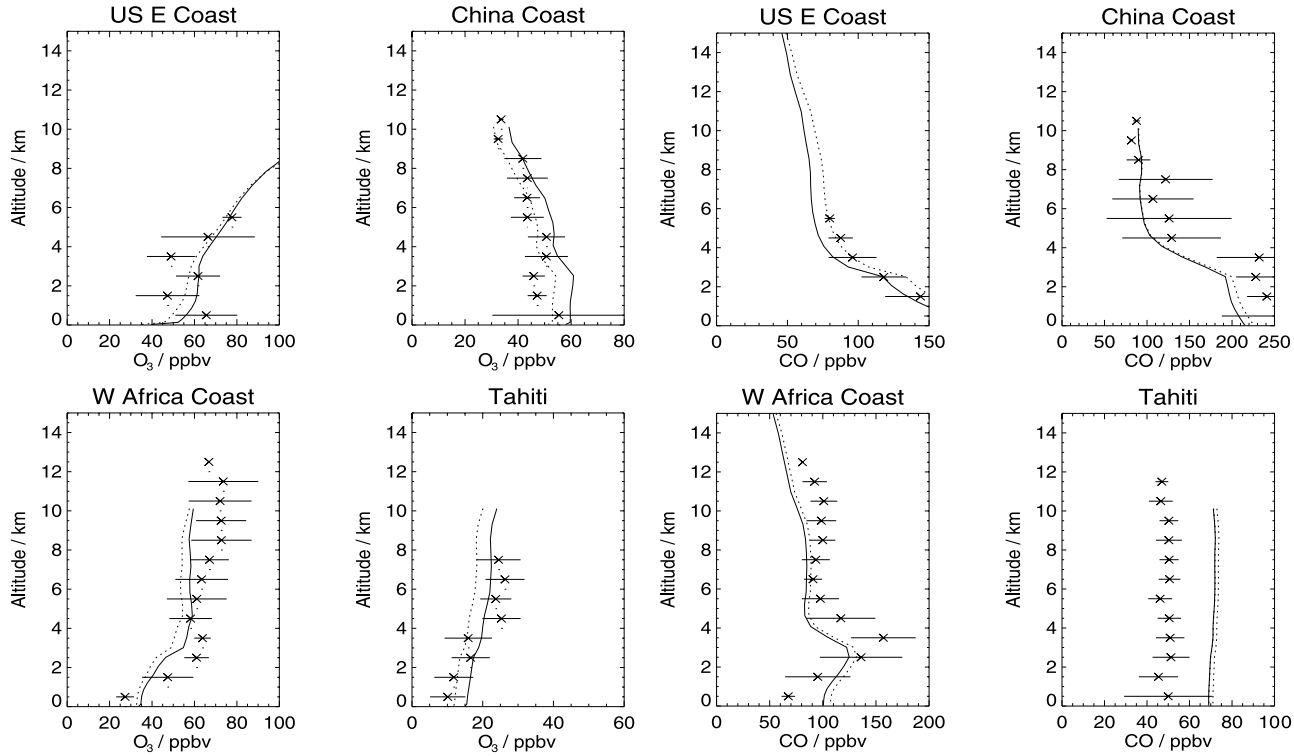

Figure 1. Comparisons of TOMCAT modeled ozone and CO profiles (ppbv) from runs **RQY** (solid line) and **OLD** (dotted line) with aircraft observations from four NASA expeditions (crosses). Locations of observations are described in Table 3. Horizontal bars show standard deviations on observations.

J loss between the studies may be a consequence of differences in strengths and locations of sources used, or the different relative strengths of surface sinks. The lack of a modeled ocean flux term also reduces our global source and sink terms relative to previous studies. However, it should be noted that if the *J* loss rate were a larger fraction of the total sink than suggested by **RQY**, any fractional reduction to the photolysis loss of acetone would produce an even more significant impact on the global acetone budget than described here.

[22] The effect of **NQY** is to reduce photolysis loss of acetone by a factor of ~2, to 9.3 Tg yr^{-1}. This results in a large increase in the OH sink, to more than 50% of the annual loss, making this the dominant tropospheric loss pathway for acetone. Dry deposition also increases to account for 21% of the loss. This significant reduction in the *J* loss decreases the overall loss rate of acetone, resulting in an increase in its atmospheric lifetime from 22 to 35 days. This leads to an overall increase in acetone concentrations globally, increasing the atmospheric burden from 2.6 to 4.1 Tg. This is a similar burden estimate to that produced by *Jacob et al.* [2002] (3.8 Tg), however **NQY** mean that it can be maintained by approximately half of the global acetone source strength used in that study.

[23] Table 7 summarizes the contributions from different altitude ranges to the total tropospheric photochemical loss of acetone for **RQY** and **NQY**. At altitudes above 500 hPa, the tropospheric destruction of acetone reduces from 11.2 Tg/yr to 9.1 Tg/yr. This results in a large increase in OH destruction of acetone from ~17 Tg/yr to ~24 Tg/yr. The absolute mass of acetone lost below 750 hPa increases by more than 2 Tg with **NQY** compared to **RQY**. Almost all of this increase is offset by reduced destruction above 500 hPa. More than 70% of acetone is destroyed in the tropics, where loss is more efficient due to larger OH concentrations and actinic flux. Fractional loss in the SH increases slightly with **NQY** compared to **RQY**, mainly at the expense of decreased fractional loss in the NH extratropical UT due to slower *J* rates. This small shift toward a larger fractional destruction in the SH is a result of larger acetone concentrations persisting in regions where efficient OH loss can consequently remove more acetone. The **OLD** and **RQY** simulations show very similar losses, except in the UT where small changes to photolysis rates slightly increase loss in the **RQY** simulation.

3.3. Comparisons With Observations

[24] We compare modeled concentrations of acetone with observations made by both aircraft and surface sites at

Table 5. CTM Surface Emission Fluxes

Species	Emissions (Tg/year)
NO_2	146
CH_4	517
CO	1770
HCHO	14
C_2H_6	16
MeCHO	0.31
C_3H_8	16
Me_2CO	27

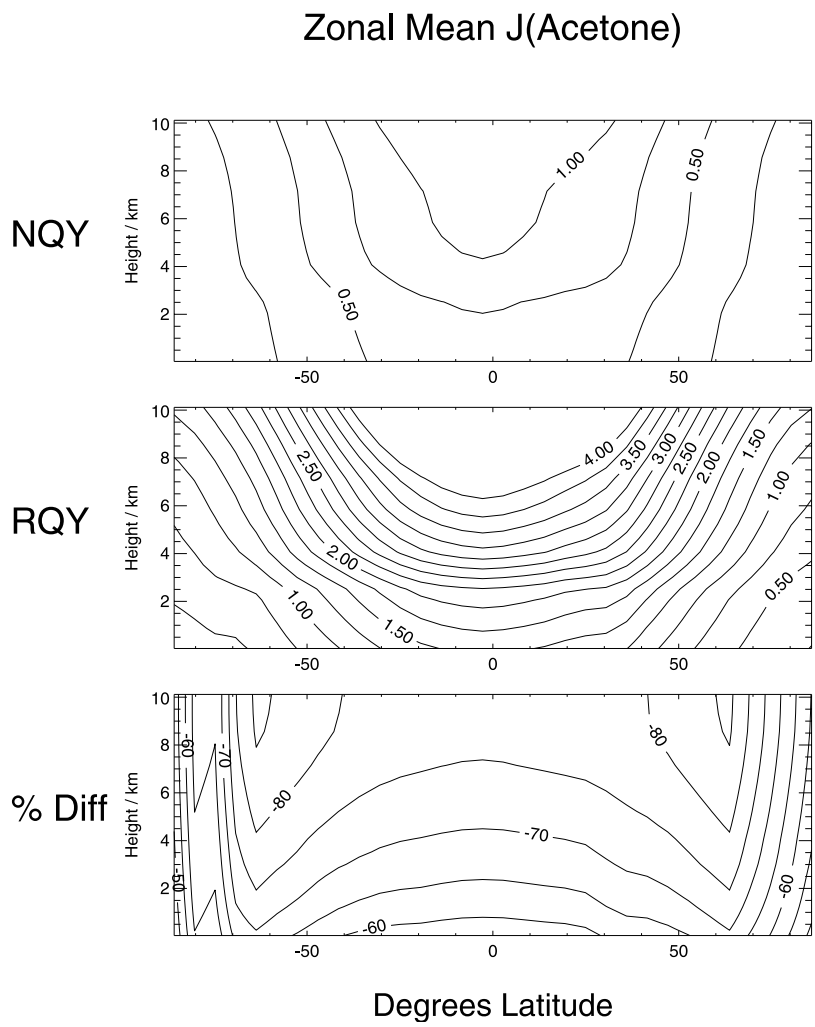

Figure 2. Zonal mean annual average acetone photolysis rates (10^{-7} s^{-1}) for TOMCAT model runs **RQY** and **NQY** and percentage difference between these runs.

various locations. Vertical profile data are composites of observations made during four NASA expeditions, binned into altitude ranges [*Emmons et al.*, 2000]. Surface concentrations are taken from *Solberg et al.* [1996]. We also compare surface concentrations of propane, the sole acetone precursor in the model. Table 8 summarizes the locations and times of year of each of the aircraft data sets used. It should be noted that these comparisons are climatological, and emissions and meteorology may not be fully appropriate for the particular time of the observations. The observations are sparse and may not necessarily be representative of the region and period considered. However, we note that PEM-Tropics B observations were made in regions remote from sources and are therefore likely to be more regionally representative.

[25] Figure 5 shows comparisons of TOMCAT with profiles of acetone observed at the locations and times listed in Table 8. Profiles of **OLD** concentrations are included to demonstrate the small changes to acetone introduced by the online photolysis treatment (**RQY**). Differences between **OLD** and **RQY** are small compared with the effects of **NQY**.

[26] Modeled acetone concentrations in the lower troposphere in the region of North American outflow (Labrador and U.S. East Coast) are small compared with those observed during the ABLE-3B experiment. Underestimations of acetone concentrations observed during this mission are also found in the MOZART [*Hauglustaine et al.*, 1988] and GEOS-CHEM [*Jacob et al.*, 2002] models. *Jacob et al.* [2002] demonstrated that their main acetone source in the PBL of the Eastern Canada region was oxidation of methylbutanol and monoterpenes. These sources are not included in TOMCAT, which may explain the large underestimation of acetone in the Labrador PBL. Underestimation of acetone in the free troposphere of the GEOS-CHEM model was attributed to anomalously high biomass burning sources during the ABLE-3B mission [*Singh et al.*, 1994]. These anomalous emissions are also absent from the TOMCAT simulation. Profiles of acetone concentrations observed in the Western Pacific during PEM-West B are generally well reproduced by the **RQY** model in the free troposphere. Concentrations in the Japan coast PBL are overestimated by TOMCAT with both **RQY** and **NQY**. Similar overestimations are seen in the MOZART model PBL in this region [*Hauglustaine et al.*, 1988]. Free tropospheric concentrations are reproduced well with **NQY** in the China and Japan coast regions but are overestimated at all altitudes for the Phillipine Sea region. *Jacob et al.* [2002] required an

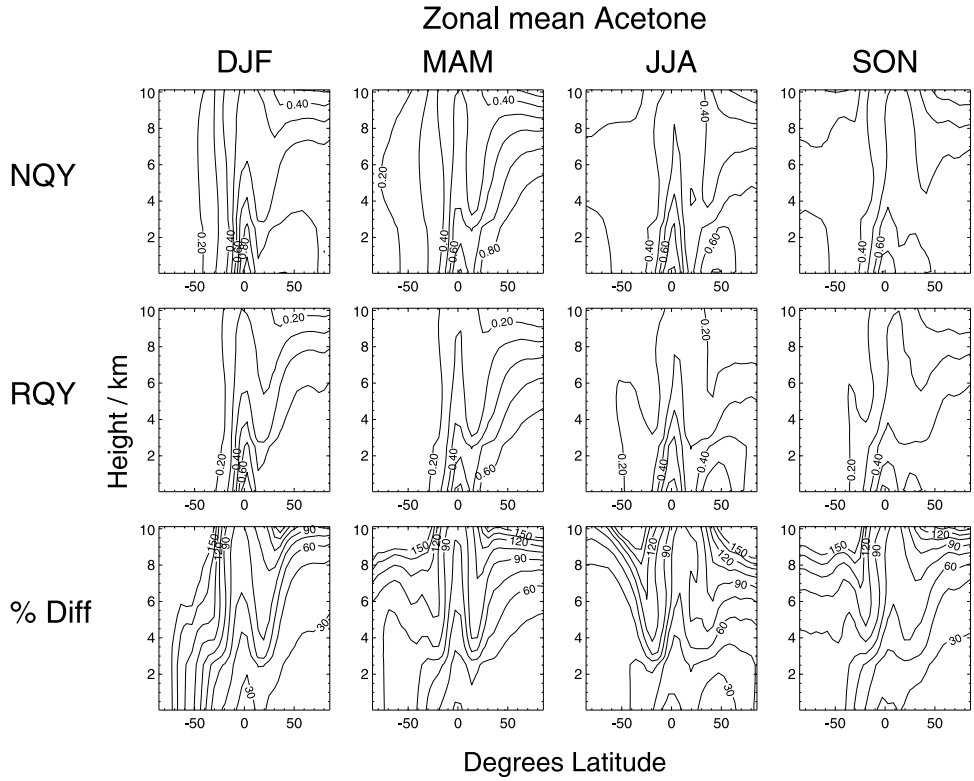

Figure 3. Zonal mean seasonal mean acetone mixing ratio (ppbv) from the surface to 10 km for DJF, MAM, JJA, and SON for TOMCAT runs **NQY** and **RQY** and the percentage difference between these runs.

increased ocean sink term to reduce acetone concentrations in the GEOS-CHEM model, in order to reproduce the PEM-West B observations. Such a sink is not included in TOMCAT, which may explain the cases of overestimation in both the PBL and free troposphere with **NQY** in this region. The **RQY** model underestimates observations made during the TRACE-A campaign at all altitudes. *Hauglustaine et al.* [1988] found a similar underestimation in the UT which they attributed to missing biomass burning sources in the region. However, the **NQY** TOMCAT run provides a much improved match to the observed acetone concentrations, with a small underestimation remaining in the UT. This may demonstrate that a large part of the discrepancy between modeled and simulated acetone concentrations in this region may be explained by the longer acetone lifetime resulting from **NQY**. Observations from the PEM-Tropics B expedition provide acetone concentrations in some of the most remote regions of the tropical Pacific. *Singh et al.* [2001] noted that the ubiquity and invariability of acetone in these regions cannot be reconciled with long-range transport from continental sources, given the accepted acetone lifetime. A large ocean source of acetone was invoked by *Jacob et al.* [2002] in order to reproduce these observations in the GEOS-CHEM model. This source contributed up to 50% of the modeled acetone concentrations at Tahiti and Easter Island. However, Figure 5 demonstrates that the increased acetone lifetime resulting from **NQY** is capable of explaining the abundances of acetone in these remote regions without the need for additional ocean sources.

[27] The general improvement in the model simulation with **NQY** is indicated by a reduction in the mean model bias relative to the aircraft observations from −50% with **RQY** to −17% with **NQY**.

[28] Comparisons of acetone and propane (the sole model acetone precursor) with observed concentrations are made for a selection of surface sites covering a range of Northern Hemisphere latitudes in Figure 6. Observations at Kosetice (Czech Republic) display a strong seasonal cycle which is also displayed to varying degrees at several other European sites. The summer maximum can be attributed to vegetative emissions and oxidation of monoterpenes [*Jacob et al.*, 2002]. Monoterpene acetone precursors are not included in TOMCAT, which may explain the underestimation of summer concentrations. Similar underestimations are seen at other European sites (e.g., Birkenes (8E, 58N) and Donon (48N, 7E) (not shown)). This seems to have less impact at the Rucava site, however. Winter concentrations are dominated by anthropogenic emissions and iso-alkane oxidation and are reproduced well at Kosetice. Despite an underestimation in propane during winter at Rucava and Zeppelin, acetone in winter is overestimated. This may suggest that anthropogenic emissions are too large or point to the lack of an ocean sink. *Jacob et al.* [2002] required such a sink to reproduce the winter minima at many of the surface sites and to capture the magnitude of acetone concentrations throughout the year at the remote Arctic site Zeppelin. However, summertime acetone at Zeppelin is well captured by TOMCAT, despite the lack of an ocean sink. We note that acetone at the Ispra site (46N, 8E) (not shown) is

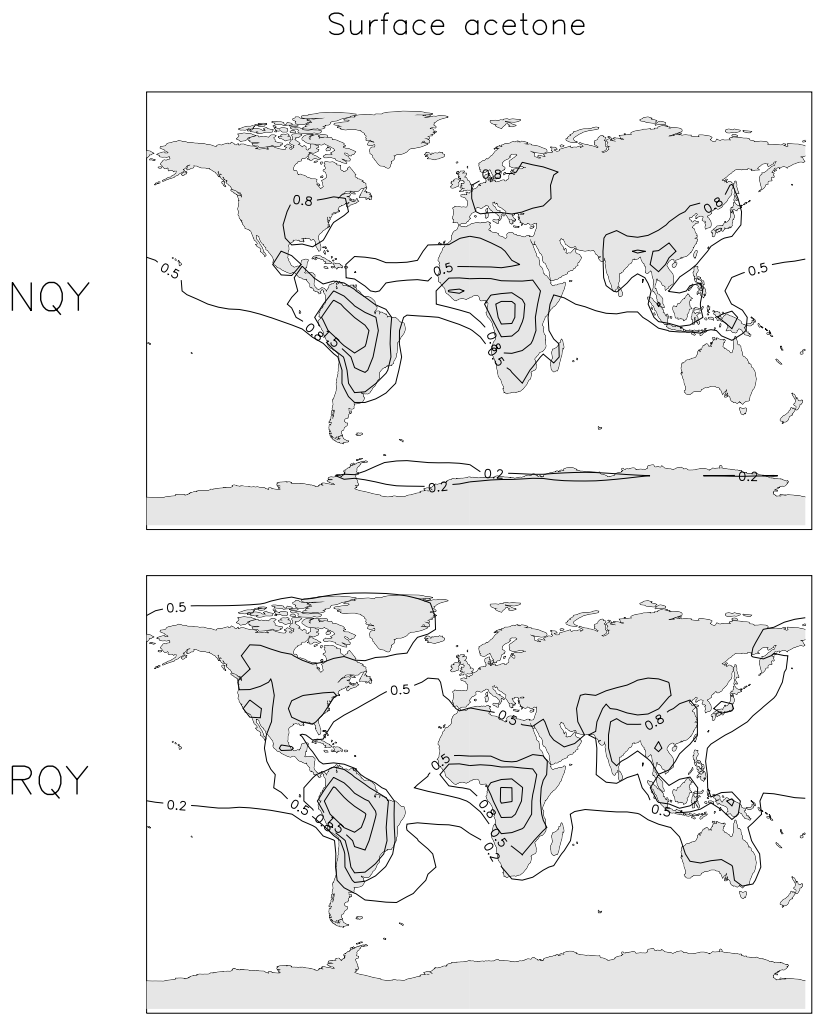

Figure 4. Surface-level annual mean acetone mixing ratio (ppbv) from TOMCAT runs **NQY** and **RQY**. Contour values are 0.1, 0.2, 0.5, 0.8, 1.5, 2.1, and 5 ppbv.

underestimated throughout the year, and the observations appear to be nonrepresentative of the region, as suggested by *Solberg et al.* [1996] and *Jacob et al.* [2002]. Acetone observations at the remote free-tropospheric site Mauna Loa are sparse; however, the magnitude of the observed concentrations is captured well by TOMCAT. Spring and summer concentrations are slightly better reproduced with **NQY**, and **RQY** give a better representation of the winter observations. The propane comparison for winter at Mauna Loa suggests that the propane acetone source may be too large in early winter.

3.4. NO_y Partitioning

[29] The peroxyacetyl radical is a product of acetone photolysis. A change in the acetone *J* rate is therefore likely to change the production of PAN and so alter the partitioning of nitrogen between the different NO_y species. A slower acetone photolysis rate may significantly reduce the production of PAN, particularly in colder regions such as the UT [*Arnold et al.*, 2004]. It should be noted that the model simulations do not include isoprene and its derivatives which are efficient in the formation of PAN. Fractional changes to PAN and NO_x are therefore likely to be somewhat different from those derived here, if isoprene chemistry were to be included. Nevertheless, the study provides an indication of the regional and global effects of reduced acetone photolysis on its interaction with NO_y.

[30] Figure 7a compares zonal mean PAN distributions using **RQY** and **NQY**. PAN concentrations in the NH are reduced overall, most significantly in the cold tropical UT, with a maximum reduction of ~12%. Maximum seasonal average PAN values of ~200 pptv occur in the springtime NH at high latitudes. These are reduced by between 10 and 17% with **NQY**.

[31] In the SH summer and autumn, PAN concentrations mostly increase with **NQY** in the extratropics. This suggests

Table 6. Annual Global Mean Acetone Budget Terms for the Three Photolysis Treatments (**OLD**, **RQY**, and **NQY**)

	OLD	RQY	NQY
τ_{acet}/days	26	22	35
Burden/Tg	3.0	2.6	4.1
Photolysis loss/Tg	17.0	18.2	9.3
OH oxidation/Tg	17.1	16.5	23.9
NO_3 oxidation/Tg	0.17	0.17	0.23
Dry deposition/Tg	7.9	7.3	8.8
Alkane source/Tg	15.5	15.5	15.5
Emissions/Tg	27.0	27.0	27.0

Table 7. Total Annual Photochemical Loss of Acetone for Different Altitude Ranges From the Three Model Runs for the Troposphere Only (Tg)

	OLD	RQY	NQY
Above 250 hPa	2.8	3.1	2.5
500–250 hPa	8.2	8.2	6.6
750–500 hPa	10.0	10.0 9.6	
Below 750 hPa	20.3	20.2	22.4

larger amounts of PAN production in regions where it is limited by the abundance of acetone. The increased acetone lifetime means that acetone concentrations in regions remote from sources (e.g., much of the extratropical SH) are larger with **NQY** allowing enhanced formation of PAN. This effect is greatest in autumn and winter where the acetone lifetime is longest and PAN is most thermally stable. The fractional increases in PAN concentrations associated with this are up to 15% in these seasons. However, the actual PAN concentrations are far smaller than in the NH.

[32] In SH spring, PAN concentrations are mostly reduced with **NQY**. This is due to PAN production being limited by the suppressed photochemical formation of peroxyacetyl radicals from acetone, rather than the transport of acetone to remote regions. This results from the more efficient springtime photo-oxidation of acetone and the smaller increase to its lifetime compared to the autumn and winter months.

[33] Distributions of NO_x show corresponding reductions and increases associated with increased and reduced formation of PAN, respectively. Zonal mean NH springtime NO_x shows the most notable increase (up to 15%) in the high latitude UT. The tropical UT shows increases to annual mean NO_x concentrations of ~5%. This is significant in perturbing the OH/HO_2 ratio, with consequences for changes in HO_x brought about by **NQY**.

3.5. HO_x and the Tropospheric Oxidizing Capacity

[34] Acetone photo-oxidation has been suggested as an important source of HO_x in the dry UT [*Singh et al.*, 1995; *Arnold et al.*, 1997; *McKeen et al.*, 1997; *Jaeglé et al.*, 2000]. Using a box model constrained with UT aircraft observations, *Arnold et al.* [2004] showed that **NQY** reduced the contribution of HO_x production from acetone photo-oxidation to the midlatitude and tropical HO_x budgets by factors of 4 and 2, respectively. Here, we discuss the impacts of **NQY** on the global distributions of HO_x over the annual cycle.

[35] Figure 8 shows that decreases to HO_x are produced in both tropospheric hemispheres with **NQY**. The largest HO_x reductions are in the NH, where acetone concentrations are dominated by the relatively large NH acetone source strength and transport to more remote regions is less important.

[36] The tropical middle/upper troposphere shows a small increase in OH with **NQY**, despite an overall decrease in HO_x. This is due to an increase in the OH/HO_2 ratio, caused by increases to NO_x (see section 3.4). Such repartitioning also occurs throughout the NH, where NO_x concentrations are more substantially enhanced, although it does not lead to an OH increase due to the larger overall decrease in HO_x.

[37] Zonal mean concentrations of HO_x in the NH winter reduce by up to ~10% in the midlatitude/high-latitude UT. In this season and region of the troposphere, the acetone photolysis rate is most significantly reduced by **NQY**. Consequently, the acetone HO_x yield in this region displays the most sensitivity to **NQY**. Fractional reductions to zonal mean HO_x in the tropical regions are up to ~4% in the UT but are far less at lower altitudes, where the reduction to the acetone J rate is smaller, and the HO_x source term is dominated by ozone photolysis.

[38] The global-scale impact of the changes to HO_x associated with **NQY** can be assessed as changes to the global mean concentration of OH, $\overline{[OH]}$, and the tropospheric oxidizing capacity. $\overline{[OH]}$ is given here in two forms, as recommended by *Lawrence et al.* [2001]. First, we have calculated the "air mass-weighted" global mean concentration of OH, $\overline{[OH]}_M$. This is the OH number density weighted by the mass of each model grid cell (M_{gc}) in the model troposphere:

$$\overline{[OH]}_M = \frac{\Sigma_{trop}\left(M_{gc}\cdot[OH]\right)}{\Sigma_{trop}M_{gc}}. \quad (1)$$

We define grid cells to be tropospheric where PV $\leq$ 2 PVU and potential temperature is less than 380 K.

[39] Second, we present the global mean OH concentration weighted by the product of the reaction rate coefficient

Table 8. Locations and Dates of Aircraft Data Sets Used to Compare With Vertical Profiles of CO, Ozone, and Acetone Concentrations From TOMCAT[a]

Region	Latitude	Longitude	Months	Mission
Labrador	50°N–55°N	300°E–315°E	Jul/Aug	ABLE-3B
U.S. East Coast	35°N–45°N	280°E–290°E	Jul/Aug	ABLE-3B
China Coast	20°N–30°N	115°E–130°E	Feb/Mar	PEM-West B
Japan	25°N–40°N	135°E–150°E	Feb/Mar	PEM-West B
Phillipine Sea	5°N–20°N	135°E–150°E	Feb/Mar	PEM-West B
Brazil, East	15°S–5°S	310°E–320°E	Sep/Oct	TRACE-A
Africa, South	25°S–5°S	15°E–35°E	Sep/Oct	TRACE-A
South Atlantic	20°S–0°S	340°E–350°E	Sep/Oct	TRACE-A
W. Africa Coast	25°S–5°S	0°E–10°E	Sep/Oct	TRACE-A
Easter Island	40°S–20°S	240°E–260°E	Mar/Apr	PEM-Tropics B
Fiji	30°S–10°S	170°E–190°E	Mar/Apr	PEM-Tropics B
Tahiti	20°S–0°S	200°E–230°E	Mar/Apr	PEM-Tropics B
Christmas Island	0°N–10°N	200°E–220°E	Mar/Apr	PEM-Tropics B
Hawaii	10°N–30°N	190°E–210°E	Mar/Apr	PEM-Tropics B

[a]For more information on data sets and missions see *Jacob et al.* [2002] and references therein.

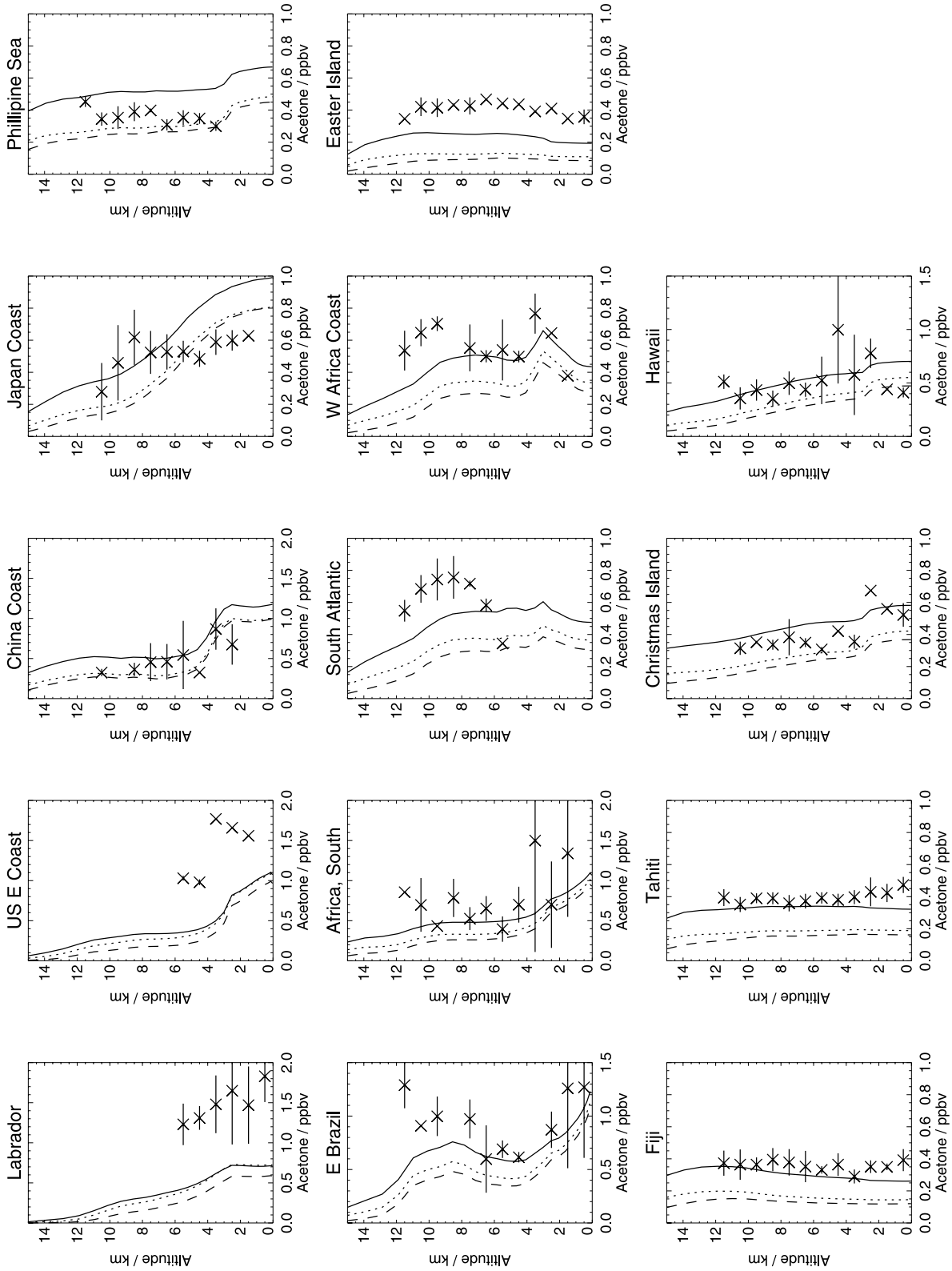

Figure 5. Comparisons of TOMCAT modeled acetone profiles (pptv) from runs **RQY** (dashed line), **NQY** (solid line), and **OLD** (dotted line) with aircraft observations from four NASA expeditions (crosses) at 15 locations described in Table 8. Horizontal bars show standard deviations on observations.

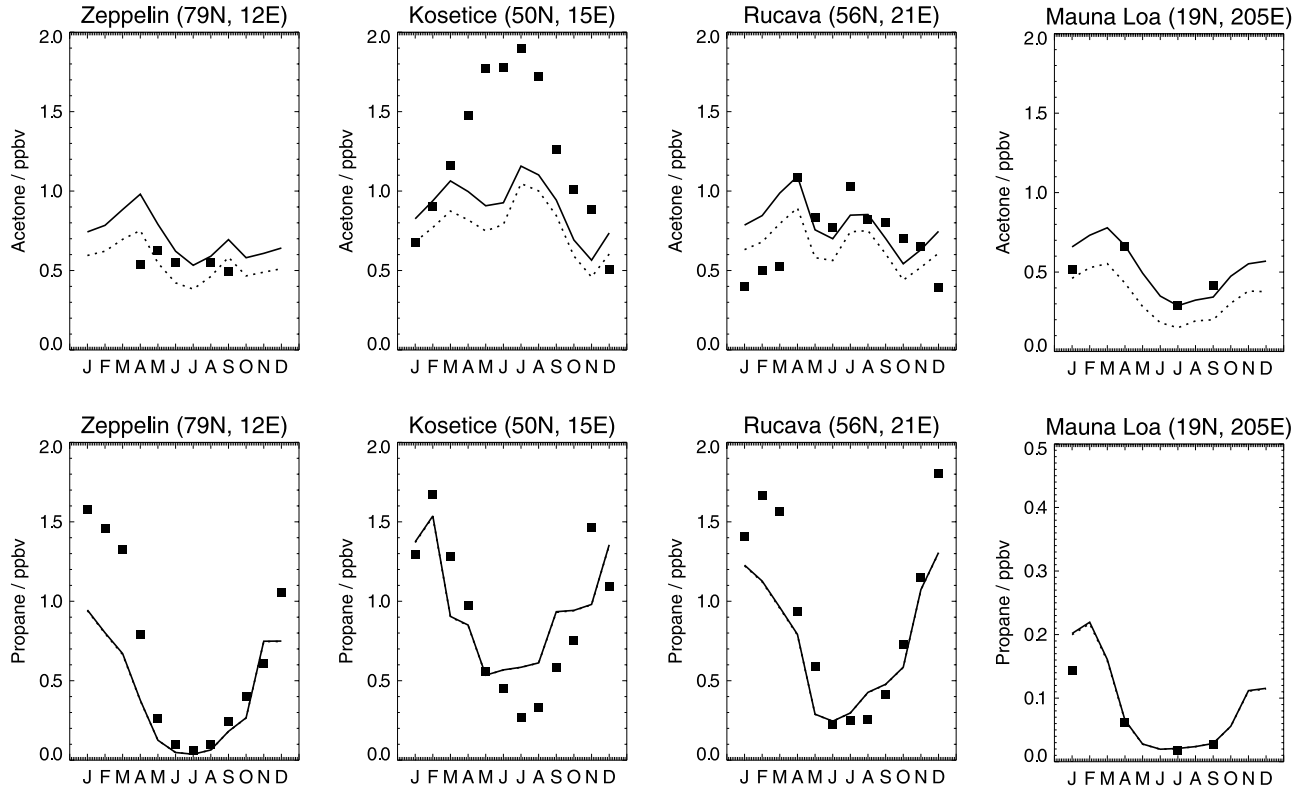

Figure 6. Comparisons of TOMCAT model acetone (top) and propane (bottom) mixing ratios (pptv) for runs **RQY** (solid line) and run **NQY** (dotted line) with those observed (symbols) at European surface sites and in the free troposphere at Mauna Loa.

for OH with methane and the mass of methane in each tropospheric model grid cell, $\overline{[OH]}_{CH_4}$:

$$\overline{[OH]}_{CH_4} = \frac{\Sigma_{trop}\left(M_{gc}.k.[CH_4][OH]\right)}{\Sigma_{trop}\left(M_{gc}.k.[CH_4]\right)}, \quad (2)$$

where k is the temperature-dependent bimolecular reaction rate coefficient for reaction of CH_4 and OH ($k = 1.85 \times 10^{-12}\exp(-1690/T)$ (http://www.iupac-kinetic.ch.cam.ac.uk)). This T-dependence impacts the capacity OH has for oxidation of gases such as methane through the troposphere. This quantity is proportional to the inverse of the global mean methane lifetime, τ_{CH_4}:

$$\tau_{CH_4} = \frac{\Sigma_{trop}\left(M_{gc}.[CH_4]\right)}{\Sigma_{trop}\left(M_{gc}.k.[OH][CH_4]\right)}. \quad (3)$$

[40] Table 9 shows these OH concentrations and τ_{CH_4} as annual means. Our mass-weighted **NQY** global mean OH of $\sim 1.03 \times 10^6$ molec cm^{-3} is within the range of recent observational estimates (1.16×10^6 molec cm^{-3} [*Spivakovsky et al.*, 2000]; 0.94×10^6 molec cm^{-3} [*Prinn et al.*, 2001]). The decrease to global mean [OH] introduced by **NQY** is on the order of 0.5%, i.e., no change to the nearest 10^4 molec cm^{-3}. This represents a relatively small change to the global annual mean methane lifetime (+0.4%). The insensitivity of the global oxidizing capacity to **NQY** partly reflects that the largest decrease to the acetone HO_x yield occurs in regions which do not contribute a significant fraction to the global HO_x burden (winter high-latitude UT), with a smaller reduction to the acetone J rate produced in the tropical UT, where acetone photolysis contributes most significantly to the global HO_x burden. In addition, increases to NO_x concentrations in the tropical UT, brought about by reduced formation of PAN, result in an increase in the OH/HO_2 ratio, which counteracts decreases in OH resulting from reduced acetone photolysis.

3.6. Ozone

[41] *Arnold et al.* [2004] showed that in the isolated UT, reduced acetone photolysis could result in an overall increase in ozone production through the maintenance of higher NO_x and acetone concentrations. However, under conditions of regular replacement of UT air by polluted NO_x-rich air (e.g., in the tropical UT), ozone production was was shown to reduce due to slower acetone photolysis, as it became limited by the yield of peroxy radicals from acetone photo-oxidation.

[42] The tropospheric ozone budget is controlled by input from the stratosphere, deposition to the surface, and photochemical production/loss. Ozone is photochemically produced in the troposphere by the photolysis of NO_2, formed by the oxidation of NO by peroxy radicals. Despite the perturbations to NO_x and reduction in efficiency of peroxy radical production from acetone in run **NQY**, changes to ozone are relatively small.

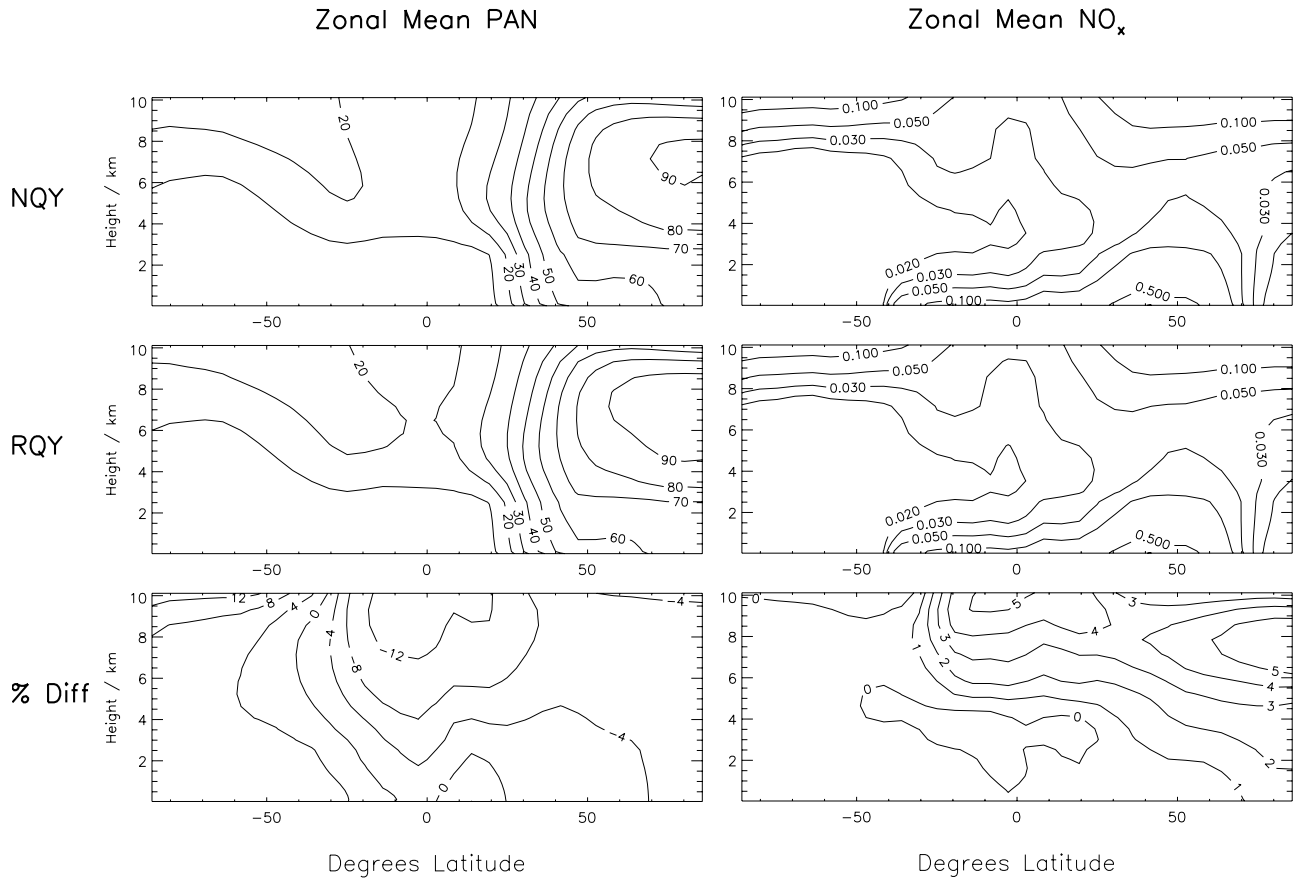

Figure 7. As Figure 3 but for PAN (pptv) and NO_x (ppbv). Contour values for NO_x are 0, 0.02, 0.03, 0.05, 0.1, 0.5, 1, and 2 ppbv.

[43] The largest change in ozone is a ~1% reduction in the extratropical lower troposphere in NH winter. UT ozone concentrations show a small enhancement at all latitudes and seasons with **NQY** compared to **RQY**, likely associated with the enhancement to NO_x concentrations resulting from reduced PAN formation.

[44] The small magnitude of the changes to global ozone introduced by **NQY** partly reflects the small magnitude of the perturbation caused to the global mean radical budget, demonstrated by the small change to global mean OH. Despite significant fractional changes to the NO_x concentrations in some seasons and locations, changes to ozone concentrations remain small. This demonstrates the strong buffering of the global photochemical term of the tropospheric ozone budget.

4. Conclusions

[45] We have used a 3-D chemical transport model to investigate the global impact of recent laboratory measurements of the temperature dependence of the acetone photolysis quantum yield [*Blitz et al.*, 2004]. The new quantum yields (**NQY**) decrease the global annual mean photolysis loss of acetone by a factor of ~2. In the cold upper troposphere (UT) the decrease is between ~80 and 90%. The atmospheric lifetime of acetone increases from 22 to 35 days, with an increase in the atmospheric burden from 2.6 to 4.1 Tg, in agreement with that derived by *Jacob et al.* [2002]. This is maintained with a global source of ~43 Tg/yr of acetone, which is approximately half the magnitude of that inferred in the inverse modeling study of *Jacob et al.* [2002]. In a note added in proof, *Singh et al.* [2004] suggested that an increased acetone lifetime due to **NQY** would reduce the acetone source strength needed to reproduce observations. This study confirms this; however, the source we require is substantially lower than previously suggested. In addition, our source of 43 Tg/yr is in good agreement with the inventory-based source strength of 56 Tg/yr, derived by *Singh et al.* [2000]. Oxidation by OH increases by ~40% and becomes the dominant loss route for acetone. Consequently, 2.3 Tg more acetone is destroyed in the lower troposphere with **NQY**, compensated for by a reduction in the loss of acetone at altitudes above 500 hPa. There are large relative changes in the remote SH due to long-range transport facilitated by the increased acetone lifetime.

[46] The general improvement in the model simulation with **NQY** is indicated by a reduction in the mean model bias relative to aircraft observations from −50% with **RQY** to −17% with **NQY**. Comparisons of model and observed acetone profiles from the remote tropical Pacific demonstrate much improved agreement with **NQY**. This provides an alternative means of reconciling model/observation discrepancies in these regions without the need to invoke a net

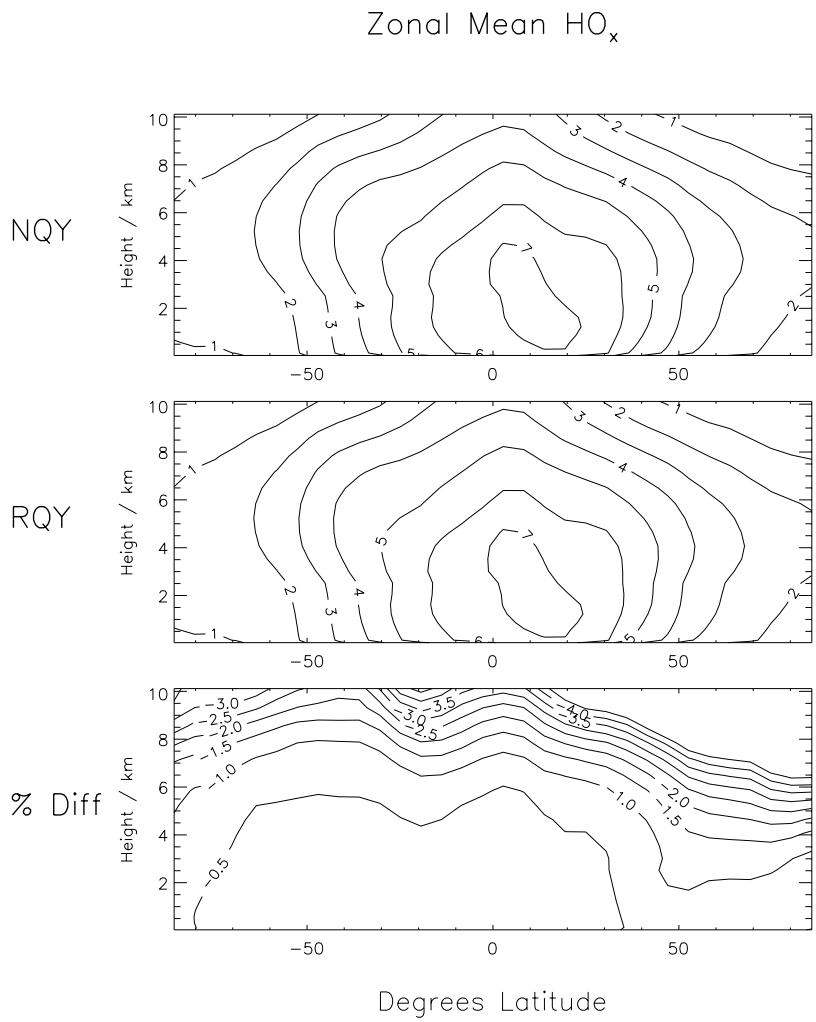

Figure 8. As Figure 3 but for HO_x (pptv).

ocean source for acetone, as has been suggested in previous studies [*Singh et al.*, 2001; *Jacob et al.*, 2002]. Our poor model agreement with the seasonality of acetone concentrations at some European surface sites, and an overestimation of acetone over the western Pacific, may suggest a role for the oceans as a net sink for acetone. However, uncertainties in model sources make a definitive conclusion difficult.

[47] The changes to the model acetone photolysis have a significant impact on NO_y species, especially PAN. With the new quantum yields PAN decreases in the cold UT and throughout the Northern Hemisphere. PAN increases are modeled in Southern Hemisphere, as the increases in acetone outweigh the slower rate of peroxyacetyl production. NO_x increases with **NQY** in regions of reduced PAN formation. The tropical UT shows increases to NO_x in all seasons.

[48] The new quantum yields reduce tropospheric HO_x(=OH + HO_2) globally. However, the impact on global model OH is small (~0.5%). This is due to the largest fractional changes to HO_x being in regions which do not contribute significantly to the global mean OH concentration, and changes to the OH:HO_2 ratio, caused by changes in NO_x. The model shows small increases in OH in the tropical UT, despite a small overall decrease in HO_x due to this repartitioning.

[49] Ozone concentrations are changed very little with **NQY**, despite relatively significant changes in NO_x and NO_y. A maximum reduction of less than 1% is modeled in the extratropical lower troposphere in NH winter. This reflects the small perturbations to the radical budget brought about by **NQY** and the strong buffering of the ozone photochemical system.

[50] Overall, the new quantum yields have large implications for our understanding of the global acetone budget. The global source strength may be up a factor 2 smaller than that derived from previous modeling studies. The revised

Table 9. Annual Global Means of OH and Corresponding CH_4 Lifetime for the Three TOMCAT Runs[a]

	OLD	RQY	NQY
$\overline{[OH]}_M/10^6$ molec cm^{-3}	0.936	1.030	1.026
$\overline{[OH]}_{CH_4}/10^6$molec cm^{-3}	1.158	1.298	1.294
τ_{CH_4}/years	8.91	7.95	7.98

[a]See text for details.

lifetime may also have reconciled previous model/observation differences in remote regions such as the tropical Pacific. This has implications for previous conclusions regarding the role of oceanic sources in the acetone budgets of these regions. The significant increase to the acetone lifetime also means that it can play a role in NO_y and HO_x chemistry in regions further from continental sources than was previously appreciated.

[51] **Acknowledgments.** This work was supported by the UK Natural Environment Research Council (NERC). We thank D. Heard and M. Pilling for comments and support. We thank D. Stevenson and N. Savage for help with the emissions. We thank D. Hauglustaine for supplying NMHC observations. The ECMWF analyses were obtained via the BADC. We acknowledge the NERC NCAS/UGAMP programme for supercomputer resources. We thank the reviewers for helpful comments.

References

Arnold, F., V. Burger, B. Droste-Fanke, F. Grimm, A. Krieger, J. Schneider, and T. Stilp (1997), Acetone in the upper troposphere and lower stratosphere: Impact on trace gases and aerosols, *Geophys. Res. Lett.*, *24*, 3017–3020.

Arnold, S. R., M. P. Chipperfield, M. A. Blitz, D. E. Heard, and M. J. Pilling (2004), Photodissociation of acetone: Atmospheric implications of temperature dependent quantum yields, *Geophys. Res. Lett.*, *31*, L07110, doi:10.1029/2003GL019099.

Blitz, M. A., D. E. Heard, M. J. Pilling, S. R. Arnold, and M. P. Chipperfield (2004), Pressure and temperature-dependent quantum yields for the photodissociation of acetone between 279 and 327.5 nm, *Geophys. Res. Lett.*, *31*, L06111, doi:10.1029/2003GL018793.

Carlier, P., H. Hannachi, and G. Mouvier (1986), The chemistry of carbonyls in the atmosphere: A review, *Atmos. Environ.*, *20*, 2079–2099.

Carver, G. D., P. D. Brown, and O. Wild (1997), The ASAD atmospheric chemistry integration package and chemical reaction database, *Comput. Phys. Comm.*, *105*, 197.

Chipperfield, M. P., D. Cariolle, P. Simon, R. Ramaroson, and D. J. Lary (1993), A three-dimensional modeling study of trace species in the Arctic lower stratosphere during winter 1989–90, *J. Geophys. Res.*, *98*, 7199–7218.

Dentener, F. D., D. S. Stevenson, J. Cofala, R. Mechler, M. Amann, P. Bergamaschi, F. Raes, and R. G. Derwent (2004), Tropospheric methane and ozone in the period 1990–2030: CTM calculations on the role of air pollutant and methane emissions controls, *Atmos. Chem. Phys. Discuss.*, *4*, 1–68.

Emmons, L. K., D. A. Hauglustaine, J.-F. Muller, M. A. Carroll, G. P. Brasseur, D. Brunner, J. Staehelin, V. Thouret, and A. Marenco (2000), Data composites of airborne observations of tropospheric ozone and its precursors, *J. Geophys. Res.*, *105*, 20,497–20,538.

Gierczak, T., J. B. Burkholder, S. Bauerle, and A. R. Ravishankara (1998), Photochemistry of acetone under tropospheric conditions, *Chem. Phys.*, *231*, 229–244.

Hauglustaine, D. A., G. P. Brasseur, S. Walters, P. J. Rasch, J.-F. Muller, L. K. Emmons, and M. A. Carroll (1988), MOZART, a global chemical transport model for ozone and related chemical tracers: 2. Model results and evaluation, *J. Geophys. Res.*, *103*, 28,291–28,335.

Holtslag, A. A. M., and B. Boville (1993), Local versus nonlocal boundary layer diffusion in a global climate model, *J. Clim.*, *6*, 1825–1842.

Hough, A. M. (1988), The calculation of photolysis rates for use in global tropospheric modelling studies, *AERE Rep. R-13259*, H.M. Stationary Off., London.

Jacob, D. J., B. D. Field, E. M. Jin, I. Bey, Q. Li, J. A. Logan, and R. M. Yantosca (2002), Atmospheric budget of acetone, *J. Geophys. Res.*, *107*(D10), 4100, doi:10.1029/2001JD000694.

Jaeglé, L., et al. (2000), Photochemistry of HO_x in the upper troposphere at northern midlatitudes, *J. Geophys. Res.*, *105*, 3877–3892.

Law, K. S., P.-H. Plantevin, D. E. Shallcross, H. L. Rogers, J. A. Pyle, C. Grouhel, V. Thouret, and A. Marenco (1998), Evaluation of modeled O_3 using Measurements of Ozone by Airbus In-Service Aircraft (MOZAIC) data, *J. Geophys. Res.*, *103*, 25,721–25,737.

Lawrence, M. G., P. Jockel, and R. von Kuhlmann (2001), What does the global mean OH concentration tell us?, *Atmos. Chem. Phys.*, *1*, 37–49.

McKeen, S. A., et al. (1997), The photochemistry of acetone in the upper troposphere: A source of odd-hydrogen radicals, *Geophys. Res. Lett.*, *24*, 3177–3180.

Müller, J.-F., and G. Brasseur (1999), Sources of upper tropospheric HO_x: A three-dimensional study, *J. Geophys. Res.*, *104*, 1705–1715.

O'Connor, F., K. S. Law, J. A. Pyle, H. Barjat, N. Brough, K. Dewey, T. Green, J. Kent, and G. Phillips (2004), Tropospheric ozone budget: Regional and global calculations, *Atmos. Chem. Phys. Discuss.*, *4*, 991–1036.

Prather, M. J. (1986), Numerical advection by conservation of second-order moments, *J. Geophys. Res.*, *91*, 6671–6681.

Prather, M. J., et al. (2001), Atmospheric chemistry and greenhouse gases, in *Climate Change 2001: The Scientific Basis*, edited by J. T. Houghton et al., pp. 881, Cambridge Univ. Press, New York.

Prinn, R. G., et al. (2001), Evidence for substantial variations of atmospheric hydroxyl radicals in the past two decades, *Science*, *292*, 1882–1888.

Sander, S. P., et al. (2003), Chemical kinetics and photochemical data for use in stratospheric modeling, Update to Evaluation no. 12, *JPL Publ. 00-3*, Jet Propulsion Lab., Pasadena, Calif.

Singh, H. B., and P. L. Hanst (1981), Peroxyacetyl nitrate (PAN) in the unpolluted atmosphere: An important reservoir for nitrogen oxides, *Geophys. Res. Lett.*, *8*, 941–944.

Singh, H. B., et al. (1994), Acetone in the atmosphere: Distribution, sources and sinks, *J. Geophys. Res.*, *99*, 1805–1819.

Singh, H. B., M. Kanakidou, P. J. Crutzen, and D. J. Jacob (1995), High concentration and photochemical fate of oxygenated hydrocarbons in the global troposphere, *Nature*, *378*, 50–54.

Singh, H. B., et al. (2000), Distribution and fate of selected oxygenated organic species in the troposphere and lower stratosphere over the Atlantic, *J. Geophys. Res.*, *105*, 3795–3806.

Singh, H. B., Y. Chen, A. Staudt, D. Jacob, D. Blake, B. Heikes, and J. Snow (2001), Evidence from the Pacific troposphere for large global sources of oxygenated organic compounds, *Nature*, *410*, 1078–1081.

Singh, H. B., et al. (2004), Analysis of the atmospheric distribution, sources, and sinks of oxygenated volatile organic chemicals based on measurements over the Pacific during TRACE-P, *J. Geophys. Res.*, *109*, D15S07, doi:10.1029/2003JD003883.

Solberg, S., C. Dye, N. Schmidbauer, A. Herzog, and R. Gehrig (1996), Carbonyls and nonmethane hydrocarbons at rural European sites from the Mediterranean to the Arctic, *J. Atmos. Chem*, *25*, 33–66.

Spivakovsky, C. M., et al. (2000), Three-dimensional climatological distribution of tropospheric OH: Update and evaluation, *J. Geophys. Res.*, *105*, 8931–8980.

Stockwell, D. Z., and M. P. Chipperfield (1999), A tropospheric chemical transport model: Development and validation of the model transport schemes, *Q. J. R. Meteorol. Soc.*, *125*, 1747–1783.

Tiedtke, M. (1989), A comprehensive mass flux scheme for cumulus parameterization in large-scale models, *Mon. Weather Rev.*, *117*, 1779–1800.

Traub, M., et al. (2003), Chemical characteristics assigned to trajectory clusters during the MINOS campaign, *Atmos. Chem. Phys.*, *3*, 459–468.

van der Werf, G. R., T. J. Randerson, J. Collatz, and L. Giglio (2003), Carbon emissions from fires in tropical and subtropical ecosystems, *Global Change Biol.*, *9*, 547–562.

Wang, K.-Y., J. A. Pyle, M. G. Sanderson, and C. Bridgeman (1999), Implementation of a convective atmospheric boundary layer scheme in a tropospheric chemistry transport model, *J. Geophys. Res.*, *104*, 23,729–23,745.

Wennberg, P. O., et al. (1998), Hydrogen radicals, nitrogen radicals, and the production of ozone in the upper troposphere, *Science*, *279*, 49–53.

S. R. Arnold and M. P. Chipperfield, School of Earth and Environment, University of Leeds, Woodhouse Lane, Leeds, LS2 9JT, UK. (sra@env.leeds.ac.uk; martyn@env.leeds.ac.uk)

M. A. Blitz, Department of Chemistry, University of Leeds, Woodhouse Lane, Leeds, LS2 9JT, UK. (markb@chemistry.leeds.ac.uk)